IEEE Access
Multidisciplinary | Rapid Review | Open Access Journal

Received January 26, 2020, accepted February 21, 2020, date of publication February 28, 2020, date of current version March 16, 2020.

Digital Object Identifier 10.1109/ACCESS.2020.2976673

Self-Calibration of Joint RF Impairments in a Loopback Wideband Transceiver

JUINN-HORNG DENG[1], (Member, IEEE), CHIA-FANG LEE[1], MENG-LIN KU[2], (Member, IEEE), AND JENG-KUANG HWANG[1], (Senior Member, IEEE)

[1]Department of Electrical Engineering, Yuan Ze University, Taoyuan 32003, Taiwan
[2]Department of Communication Engineering, National Central University, Chungli 32001, Taiwan

Corresponding author: Juinn-Horng Deng (jh.deng@saturn.yzu.edu.tw)

This work was supported by the Ministry of Science and Technology, China, under Grant MOST 106-2218-E-155-006.

ABSTRACT This research studied transmitter/receiver (TX/RX) wideband (WB) RF impairments, namely frequency-dependent, frequency-independent I/Q imbalances and DC I/Q offsets. A real-based parallel structure is proposed to estimate and calibrate TX/RX WB RF impairment factors. RX impairment estimation and compensation are performed first using a frequency offset BPSK training signal. Then, the TX impairments are calibrated using a QPSK training signal. The proposed methods exhibited the following successes. First, a commercial off-the-shelf (COTS) AD9371 RF module with impairments was calibrated. After TX/RX calibration, the improvement of error vector measurement (EVM) of an OFDM 64QAM test signal was approximately 9.42 dB. Second, for the Taiwan Industrial Technology Research Institute's WB RF module with impairments, the EVM of an OFDM 16QAM test signal was calibrated and increased by about 20 dB. In summary, the proposed techniques can overcome WB RF impairments and enable high-quality WB communication.

INDEX TERMS Calibration procedures, DC I/Q offsets, frequency-dependent I/Q imbalance, frequency-independent I/Q imbalance, RF impairment.

I. INTRODUCTION

Direct up/down RF chipsets are commonly used in wideband (WB) communication systems such as the 5G mobile communication system and digital video broadcasting systems. These chipsets have advantages such as low cost, simple design, and small area. However, for direct up/down conversion, multiple RF chips and oscillation circuits induce the different impairments including I/Q imbalance, DC offset, transmitter and receiver nonlinearities, phase noise, and coupling effects. In these impairments, many studies have extensively discussed I/Q imbalance. WB communication systems incur two I/Q imbalance effects: frequency-independent and frequency-dependent I/Q imbalances. Specifically, RF local oscillators generate I and Q carriers with amplitude and phase imbalance effects, resulting in so-called frequency-independent I/Q imbalance. In WB systems, the I and Q channels have the different impulse response effects and exhibit frequency-selective distortion, which is called frequency-dependent I/Q imbalance. The aforementioned impairments occur at both the transmitter (TX) and receiver (RX) sides of a WB RF system. To overcome these impairments, we studied the feasible TX/RX loopback calibration procedures with the estimation of impairment model parameters and associated calibration parameters. In this study, digital signal processing techniques were employed to estimate RF impairments and compensate for WB RF distortion. Many researchers have studied the factors of WB RF imperfection and related compensation methods. Li *et al.* [1] proposed a low-cost envelope detector method for I/Q imbalance compensation. This method only compensates for the frequency-dependent I/Q imbalance at the TX. Hsu and Sheen [2] studied joint calibration methods for TX/RX RF impairments. They used a frequency offset (FO) method for joint TX/RX calibration. Ding *et al.* [3] proposed a real-based filter structure for the calibration of a TX with impairments. Li [4] studied I/Q imbalance modeling, estimation, and compensation and adopted complex calibration schemes to compensate for RF impairments. Luo *et al.* [5] proposed joint calibration for TX/RX RF impairments, which was only studied frequency-independent I/Q imbalances. In [6], a novel calibration scheme for

The associate editor coordinating the review of this manuscript and approving it for publication was Nagendra Prasad Pathak.

solving TX RF gain, phase, and offset problems was studied; however, frequency-selective I/Q imbalance effects were not studied. Zhang *et al.* [7] studied an iterative decision–feedback RX to compensate for I/Q imbalance. However, they did not consider a loopback calibration scheme. In [8], a WB OFDM system with frequency-dependent I/Q imbalance effects was studied. Because OFDM systems are sensitive to frequency-dependent I/Q imbalance, Matsui *et al.* proposed a blind compensation method, namely the constant modulus algorithm, to calculate the filter coefficients for compensating for frequency-dependent I/Q imbalances. Lopez-Estraviz *et al.* [9] proposed an OFDM pre-compensation technique for a TX. They used a low-complexity ML equalizer to study TX/RX frequency-dependent I/Q imbalances and propagation channel effects. A pilot signal was used to estimate the channel and I/Q imbalance coefficients. An advanced equalizer was used to compensate for the frequency-dependent I/Q imbalance. Many papers have proposed adaptive calibration methods. In [10], Cavers *et al.* proposed an adaptive compensation technique for quadrature modulation of TX RF. Lim *et al.* [11] proposed digital adaptive algorithms and used two finite impulse response filters to compensate for the gain and phase of I/Q modulators. Moreover, numerous studies have proposed digital preprocessing methods. Marchesani *et al.* [12] proposed a digital preprocessing method to compensate for the RF impairments of quadrature modulators and to improve system performance. Joint algorithms have been used to compensate for RF impairments with high distortion effects (e.g., I/Q imbalance, coupling, multiple antennas, and nonlinear factors) [13]–[15]. In [13], Anttila *et al.* proposed joint least squares (LS) methods to overcome RF I/Q imbalances and the nonlinearity of the power amplifier (PA). Gregorio *et al.* [14] studied joint calibration schemes to compensate for RF impairments at a TX with an I/Q imbalance, nonlinear PA, and crosstalk coupling effects. Moreover, Khan *et al.* [15] proposed digital preprocessing techniques at the TX for joint mitigation of I/Q imbalances and nonlinear multiple input multiple output (MIMO) PA effects.

Many studies [1], [3], [6] have proposed methods for combating WB RF imperfection distortion. However, most have examined only TX impairments and ignored RX impairments in the case of TX/RX RF loopback. Some studies [2]–[5] performed only theoretical derivation for RF impairment calibration and did not use real RF hardware to verify the proposed algorithms. Here, we examine joint calibration techniques for TX/RX impairments in a real-world loopback transceiver scenario. Note that the joint consideration of RX impairments in the TX/RX RF loopback is much more challenging than the existing works which merely concern the TX RF impairment. To achieve the loopback calibration, a real-based parallel structure is proposed to estimate and compensate the TX/RX RF impairment. We first use an FO-based BPSK training signal to estimate RX impairments and compensate for RX distortion. We subsequently calibrate the TX impairment by using a QPSK training signal. The proposed techniques were used at Taiwan's Industrial Technology Research Institute (ITRI) on the institute's own RF IC to calibrate RF impairments and improve RF performance. First, an all-digital simulation platform was developed to emulate WB RF imperfections and to design estimation and compensation technologies. Next, a WB RF module (i.e., the AD9371 RF module) and a WB instrument platform (i.e., NI PXIe-1075 5646R) were used to generate WB RF impairments. The module was used to integrate the software platform to verify the performance of the proposed calibration techniques. For the ITRI WB RF module, the proposed calibration procedures, which provided reliable performance, can be used to achieve WB signal communication.

To the best of our knowledge, none of previous studies have considered a self-calibration design for a loopback transceiver with dual real-based parallel structures for mitigating WB TX/RX RF impairments. The main contributions of this paper are as follows:

1) The structures of dual parallel real-based compensation, in which complex signals with real and imaginary parts are transformed into two parallel real signals, are proposed to effectively estimate and calibrate the TX/RX WB RF impairment effects.
2) For self-calibration of loopback transceiver, we propose that RX-side RF impairment is compensated by first using an FO-based BPSK training signal to avoid TX-side impairment effects. Second, we calibrate the TX-side RF impairments via a QPSK training signal under the RX-side RF with impairments calibration.
3) The TX- and RX-side calibration schemes has been successfully applied to compensate for RF impairments in the AD9371 and ITRI RF modules. Single-tone and OFDM test signals in two RF modules were employed to validate the performances of the improvement in the image rejection ratio (IMRR) and error vector measurement (EVM). Thus, the proposed loopback self-calibration algorithms were realized and implemented for compensation in the WB RF TX/RX IC.

The following conventions are used throughout the paper. Uppercase and lowercase boldface letters represent matrices and vectors, respectively. For matrix $\mathbf{A}$, $\mathbf{A}^T$ and $\mathbf{A}^H$ represent its transpose and conjugate transpose, respectively. The symbol $\mathbf{A}^\dagger$ denotes the pseudo inversion of $\mathbf{A}$, that is, $\left(\mathbf{A}^H\mathbf{A}\right)^{-1}\mathbf{A}^H$; $\otimes$ denotes a convolution operation; and $(\cdot)^*$ denotes a conjugate operation.

II. COMPLEX DATA MODELS OF WB TX/RX RF IMPAIRMENT COMPENSATION STRUCTURES

We consider a WB TX data model for a scenario in which the transmitted signal involves RF impairment effects, such as frequency-independent I/Q imbalance, frequency-dependent I/Q imbalance, or DC I/Q offset. A schematic of the TX signal model including the DC I/Q impairments, impairment parameters estimation, and compensation structures is depicted in Fig. 1. The transmitted baseband signal $x(n)$ can

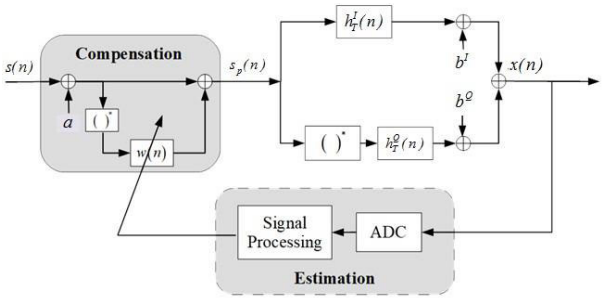

FIGURE 1. WB RF impairment and compensation structure of the TX.

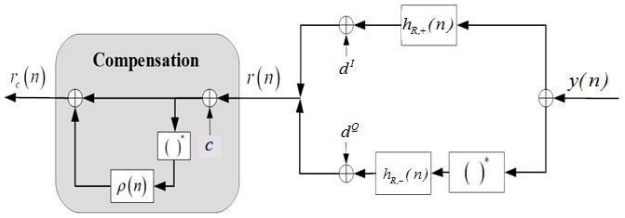

FIGURE 2. WB RF impairment and compensation structures of the RX.

be expressed using the radio impairment model as follows [4]:

$$x(n) = h_{T,+}(n) \otimes s_p(n) + h_{T,-}(n) \otimes s_p(n)^* + b \quad (1)$$

where $s_p(n)$ is the ideal baseband signal $s(n)$ passing through the calibration preprocessing, $h_{T,\pm}(n)$ is the WB RF impairment factor of the TX, $b = b^I + j \cdot b^Q$ is the TX DC I/Q offset, and $\otimes$ represents convolution operation. The parameter $h_{T,\pm}(n)$ can be expressed as follows:

$$h_{T,\pm}(n) = \frac{1}{2} \cdot \left[h_T^I(n) \pm \alpha_T e^{j\theta_T} h_T^Q(n) \right] \quad (2)$$

where $h_T^I(n)$ and $h_T^Q(n)$ are the low-pass responses of the I and Q channels, respectively, which result in a frequency-dependent I/Q imbalance. Frequency-independent I/Q imbalances, namely I/Q amplitude α_T and phase θ_T imbalances, coexist in the TX RF.

In (1), $s_p(n)$ is the discrete signal output from the preprocessing filter and is given as follows:

$$s_p(n) = [s(n) + a] + w(n) \otimes [s(n) + a]^* \quad (3)$$

where $w(n)$ is the preprocessing filter and a is the precompensated DC offset. Moreover, by substituting (3) into (1), the TX signal with the preprocessing calibration can be rewritten as follows:

$$\begin{aligned} x_p(n) &= h_{T,+}(n) \otimes \left[s(n) + a + w(n) \otimes s^*(n) + w(n) \otimes a^* \right] \\ &\quad + h_{T,-}(n) \otimes \left[s(n) + a + w(n) \otimes s^*(n) + w(n) \otimes a^* \right]^* + b \end{aligned} \quad (4)$$

The preprocessing parameters (i.e., $w(n)$ and a) are derived in Section III-A.

The WB RF impairment and the postprocessing compensation structure at the RX are depicted in Fig. 2 [2].

The RX structure uses the received signal $y(n)$ with the intentional FO μ. Thus, the loopback between the TX and RX with the FO signal can be expressed as $y(n) = e^{j2\pi\mu n} \cdot x(n)$. The purpose of this intentional FO is to estimate the RX impairment parameters, which are detailed in Section III-B. The FO-based RX signal with WB impairments in Fig. 2 can be expressed as follows:

$$r(n) = h_{R,+}(n) \otimes y(n) + h_{R,-}(n) \otimes y^*(n) + d \quad (5)$$

where $h_{R,\pm}(n)$ is the WB RF impairment factor of the RX and $d = d^I + jd^Q$ is the RX DC offset. The parameter $h_{R,\pm}(n)$ can be expressed as follows:

$$h_{R,\pm}(n) = \frac{1}{2} \left(h_R^I(n) \pm \alpha_R e^{\mp j\theta_R} h_R^Q(n) \right) \quad (6)$$

where $h_R^I(n)$ and $h_R^Q(n)$ are the low-pass responses of the I and Q channels of the RX frequency-dependent imbalance, respectively. Frequency-independent imbalances, namely gain imbalance α_R and phase imbalance θ_R, coexist in the RX. The RX signal passes through the postprocessing filter $\rho(n)$ and the compensated DC offset c. The output signal $r_c(n)$ is given as follows:

$$\begin{aligned} r_c(n) &= (r(n) - c) - \rho(n) \otimes (r(n) - c)^* \\ &= \left\{ h_{R,+}(t) - \rho(n) \otimes h_{R,-}^*(t) \right\} \otimes y(n) \\ &\quad + \left\{ h_{R,-}(t) - \rho(n) \otimes h_{R,+}^*(t) \right\} \otimes y^*(n) \\ &\quad + \left\{ \Delta_d - \rho(n) \otimes \Delta_d^* \right\} \end{aligned} \quad (7)$$

where $\Delta_d = d - c$. In Section III-B, the compensation parameters ($\rho(n)$ and c) are derived to optimize calibration performance at the RX.

III. DEVELOPMENT OF LOOPBACK TX/RX IMPAIRMENT ESTIMATION AND CALIBRATION SCHEME

A novel loopback calibration scheme is proposed for a WB RF TX/RX with impairment effects. A schematic of the proposed loopback TX/RX calibration system with real-based parallel structures is displayed in Fig. 3. Based on the real-based parallel structures, the joint TX/RX impairment effects can be elegantly separated and compensated by the proposed FO-based BPSK training signals with the individual convolution operation for each real-based impairment parameters. In what follows, we elaborate the construction of this loopback TX/RX calibration system and the related parameter estimation.

The TX/RX calibration scheme involves the following topics. First, impairment parameter estimation and preprocessing algorithms are implemented for only TX calibration. Second, postprocessing schemes compensate for RX impairment effects, and loopback TX/RX calibration procedures compensate for the overall RF impairments.

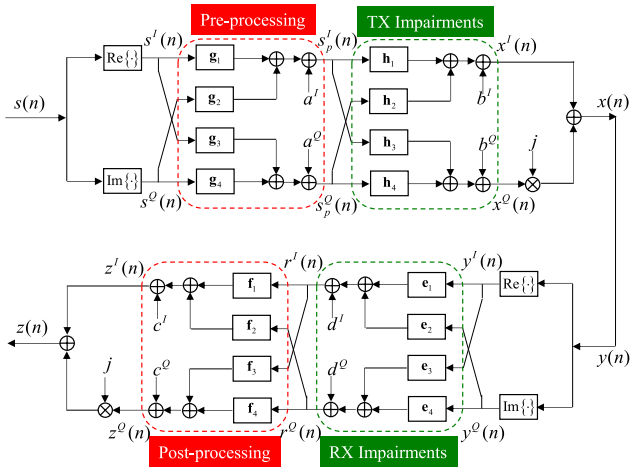

FIGURE 3. Block diagram of calibrations and impairments of the loopback TX/RX system.

A. PARALLEL FILTER DESIGN FOR IMPAIRMENT PARAMETER ESTIMATION AND PREPROCESSING CALIBRATION OF WB RF TX

In this subsection, we examine the parallel filters designed for preprocessing calibration at the TX. According to the TX data model presented in Section II, the QPSK training signal $s(n)$ is employed to estimate the impairment factors of the TX WB RF. Then, parallel preprocessing filter parameters are determined using an LS algorithm. In the following text, the design flows are introduced. First, as displayed in Fig. 3, we employ a real-based parallel structure with independent I and Q branches [3] to express a complex TX impairment signal in (1). Moreover, the TX signal of the real-based parallel structure can be derived from the complex TX signal as follows:

$$\begin{aligned} x(n) &= x^I(n) + jx^Q(n) \\ &= h_{T,+}(n) \otimes \left(s_p^I(n) + js_p^Q(n)\right) \\ &\quad + h_{T,-}(n) \otimes \left(s_p^I(n) - js_p^Q(n)\right) + \left(b^I + jb^Q\right) \end{aligned} \tag{8}$$

Here, the separated TX I and Q signals are as follows:

$$\begin{aligned} x^I(n) &= h_1(n) \otimes s_p^I(n) + h_2(n) \otimes s_p^Q(n) + b^I \\ x^Q(n) &= h_3(n) \otimes s_p^I(n) + h_4(n) \otimes s_p^Q(n) + b^Q \end{aligned} \tag{9}$$

The four real-based parallel filters are expressed as follows:

$$\begin{aligned} h_1(n) &= h_T^I(n), \quad h_2(n) = -\alpha_T \sin\theta_T h_T^Q(n) \\ h_3(n) &= 0, \quad h_4(n) = \alpha_T \cos\theta_T h_T^Q(n) \end{aligned} \tag{10}$$

Moreover, by considering the initial TX block diagram in Fig. 3 and bypassing the preprocessing block $s_p(n) = s(n)$, we can exploit the training signals $s^I(n)$ and $s^Q(n)$ in the $L_t \times 1$ vector to estimate the real-based parallel impairment parameters. The parameter L_t represents the length of the TX data. The vector form of the TX signal is expressed as follows:

$$\mathbf{x}^I(n) = \mathbf{S}^I(n) \cdot \mathbf{h}_1 + \mathbf{S}^Q(n) \cdot \mathbf{h}_2 + \mathbf{1} \cdot b^I \tag{11}$$

$$\mathbf{x}^Q(n) = \mathbf{S}^I(n) \cdot \mathbf{h}_3 + \mathbf{S}^Q(n) \cdot \mathbf{h}_4 + \mathbf{1} \cdot b^Q \tag{12}$$

where $\mathbf{1}$ is the all-one vector and $\mathbf{S}^I(n)$ and $\mathbf{S}^Q(n)$ are the Toeplitz matrices of $s^I(n)$ and $s^Q(n)$, respectively. In (11) and (12), the vectors $\mathbf{h}_i$ where $i = 1, \cdots, 4$, are the responses of $h_i(n)$. The real-based impairment parameters can be estimated through the LS method as follows:

$$\begin{aligned} \left[\hat{b}^I \quad \hat{\mathbf{h}}_1^T \quad \hat{\mathbf{h}}_2^T\right]^T &= \mathbf{S}_{LS}^{\dagger}\mathbf{x}^I \\ \left[\hat{b}^Q \quad \hat{\mathbf{h}}_3^T \quad \hat{\mathbf{h}}_4^T\right]^T &= \mathbf{S}_{LS}^{\dagger}\mathbf{x}^Q \end{aligned} \tag{13}$$

where $\mathbf{S}_{LS} = \left[\mathbf{1} \;\; \mathbf{S}^I(n) \;\; \mathbf{S}^Q(n)\right]$ is the known training signal matrix and $(\cdot)^{\dagger}$ is the pseudoinverse operation.

After the estimation of the impairment parameters, the preprocessing compensation block in Fig. 3 is activated. Thus, the preprocessing filters and the pre-calibrating DC offset must be calculated to compensate for the RF impairment effects. Moreover, according to the real-based parallel impairment structure, the symmetric structure of the real-based parallel preprocessing design is studied in Fig. 3. The preprocessing filters and the pre-calibrating DC offset are denoted by $g_i(n)$, $i = 1, \cdots, 4$ and $a = a^I + ja^Q$, respectively. We next describe the estimation of the preprocessing parameters. First, the relationship between the preprocessing DC offset a and RF impairments, i.e., $s_p(n) = a$ being compensated in (8)-(9) to acquire no DC offset $x(n) = 0$, can be written as follows:

$$\begin{aligned} a^I \cdot \mathbf{1}^T \cdot \mathbf{h}_1 + a^Q \cdot \mathbf{1}^T \cdot \mathbf{h}_2 + b^I &= 0 \\ a^I \cdot \mathbf{1}^T \cdot \mathbf{h}_3 + a^Q \cdot \mathbf{1}^T \cdot \mathbf{h}_4 + b^Q &= 0 \end{aligned} \tag{14}$$

After the impairment parameters in (13) are determined, the preprocessing DC offset a can be estimated as follows:

$$\begin{bmatrix} \hat{a}^I \\ \hat{a}^Q \end{bmatrix} = \begin{bmatrix} \sum_{n=0}^{L-1} h_1(n) & \sum_{n=0}^{L-1} h_2(n) \\ \sum_{n=0}^{L-1} h_3(n) & \sum_{n=0}^{L-1} h_4(n) \end{bmatrix}^{-1} \begin{bmatrix} -b^I \\ -b^Q \end{bmatrix} \tag{15}$$

After the DC offset is compensated by (14)-(15), the parallel preprocessing filters $g_i(n)(i = 1, \cdots, 4)$ calibrate the parallel impairment effects. Thus, the transmitted I and Q signals in (9) can be rewritten as follows:

$$\begin{aligned} x^I(n) &= h_1(n) \otimes \left(g_1(n) \otimes s^I(n) + g_2(n) \otimes s^Q(n)\right) \\ &\quad + h_2(n) \otimes \left(g_3(n) \otimes s^I(n) + g_4(n) \otimes s^Q(n)\right) \end{aligned} \tag{16}$$

$$\begin{aligned} x^Q(n) &= h_3(n) \otimes \left(g_1(n) \otimes s^I(n) + g_2(n) \otimes s^Q(n)\right) \\ &\quad + h_4(n) \otimes \left(g_3(n) \otimes s^I(n) + g_4(n) \otimes s^Q(n)\right) \end{aligned} \tag{17}$$

To calculate the values of the four real-based filters $g_i(n)$, $i = 1, \cdots, 4$, the $s^I(n)$ and $s^Q(n)$ signals are separated to express the TX signals. Thus, the following equation is obtained:

$$\begin{aligned} x^I(n) &= (h_1(n) \otimes g_1(n) + h_2(n) \otimes g_3(n)) \otimes s^I(n) \\ &\quad + (h_1(n) \otimes g_2(n) + h_2(n) \otimes g_4(n)) \otimes s^Q(n) \end{aligned} \tag{18}$$

$$x^{Q}(n) = (h_3(n) \otimes g_1(n) + h_4(n) \otimes g_3(n)) \otimes s^{I}(n) + (h_3(n) \otimes g_2(n) + h_4(n) \otimes g_4(n)) \otimes s^{Q}(n) \tag{19}$$

To calibrate impairment, the $s^I(n)$ signal in (18) is retained, and the $s^I(n)$ signal in (19) is suppressed. Thus, the following equation is obtained:

$$\begin{aligned} h_1(n) \otimes g_1(n) + h_2(n) \otimes g_3(n) &= \delta(n) \\ h_3(n) \otimes g_1(n) + h_4(n) \otimes g_3(n) &= 0 \end{aligned} \tag{20}$$

By exploiting the Toeplitz matrix $\mathbf{H}_i(n)$ of $h_i(n)$, $i = 1, \cdots, 4$ (20) can be rewritten as follows:

$$\begin{aligned} \mathbf{H}_1 \cdot \mathbf{g}_1 + \mathbf{H}_2 \cdot \mathbf{g}_3 &= \boldsymbol{\delta} \\ \mathbf{H}_3 \cdot \mathbf{g}_1 + \mathbf{H}_4 \cdot \mathbf{g}_3 &= \mathbf{0} \end{aligned} \tag{21}$$

where $\boldsymbol{\delta} = \begin{bmatrix} 1 & 0 & \cdots & 0 \end{bmatrix}^T$ is the delta vector function and vectors $\mathbf{g}_i$, $i = 1, \cdots, 4$, are the responses of $g_i(n)$. Through the LS method, the preprocessing filters $\mathbf{g}_1$ and $\mathbf{g}_3$ can be calculated as follows:

$$\begin{bmatrix} \hat{\mathbf{g}}_1 \\ \hat{\mathbf{g}}_3 \end{bmatrix} = \mathbf{H}^{\dagger} \begin{bmatrix} \boldsymbol{\delta} \\ \mathbf{0} \end{bmatrix} \quad \text{with } \mathbf{H} = \begin{bmatrix} \mathbf{H}_1 & \mathbf{H}_2 \\ \mathbf{H}_3 & \mathbf{H}_4 \end{bmatrix} \tag{22}$$

Similarly, the $s^Q(n)$ signal in (19) is retained, and the $s^Q(n)$ signal in (18) is suppressed. Thus, the following equation is obtained:

$$\begin{aligned} h_1(n) \otimes g_2(n) + h_2(n) \otimes g_4(n) &= 0 \\ h_3(n) \otimes g_2(n) + h_4(n) \otimes g_4(n) &= \delta(n) \end{aligned} \tag{23}$$

Then, the preprocessing filters $\mathbf{g}_2$ and $\mathbf{g}_4$ can be estimated using the convolutional matrix $\mathbf{H}$ as follows:

$$\begin{bmatrix} \hat{\mathbf{g}}_2 \\ \hat{\mathbf{g}}_4 \end{bmatrix} = \mathbf{H}^{\dagger} \begin{bmatrix} \mathbf{0} \\ \boldsymbol{\delta} \end{bmatrix} \tag{24}$$

B. PARALLEL FILTER DESIGN FOR IMPAIRMENT PARAMETER ESTIMATION AND POSTPROCESSING CALIBRATION OF LOOPBACK-BASED RX WB RF

In Section III-A, the preprocessing design to calibrate TX RF impairments is presented. In this section, we propose RX calibration schemes and loopback calibration procedures. In the loopback TX/RX scenario, to calibrate only the RX RF impairments, we must isolate the TX RF impairment effects; that is, we must avoid the image imbalance signal at the TX. To achieve this isolation, the BPSK training signal is transmitted by the TX; then, the signal with intentional FO (i.e., FO-based BPSK signal) is acquired to perform only RX calibration. After the RX impairments are calibrated, the TX impairments are calibrated by Section III-A to complete loopback calibration.

We propose that RX impairments are estimated first and calibration parameters are subsequently designed to compensate for the RX impairments. The process is introduced in the following. First, the BPSK signal $s(n) = s^I(n) + j0$ is used as a TX training sequences. Then, in the loopback between the TX and RX with the intentional FO μ, the RX signal and FO-based BPSK signal can be acquired to estimate the RX impairments and calibration parameters. Therefore, when using the BPSK signal $s_p(n) = s^I(n)$ in the initial TX mode in Fig. 3, the TX signal in (8) can be written as follows:

$$\begin{aligned} x(n) &= h_{T,+}(n) \otimes s^I(n) + h_{T,-}(n) \otimes s^I(n) + b \\ &= h_T^I(n) \otimes s^I(n) + b \end{aligned} \tag{25}$$

where $h_T^I(n) = h_{T,+}(n) + h_{T,-}(n)$ according to (2) and $h_T^I(n)$ is the real-part impulse response, which cannot induce a TX image imbalance effect. Thus, for simplicity, $h_T^I(n)$ is ignored in the following design. The TX signal is given by $x(n) = s^I(n) + b$, and the TX DC offset is $b = b^I + jb^Q$.

The RX signal with the intentional FO can be written as

$$y(n) = e^{j2\pi\mu n} \cdot x(n) \tag{26}$$

By substituting $x(n) = s^I(n) + b$ into (26), the RX I and Q signals $y(n) = y^I(n) + j \cdot y^Q(n)$ can be rewritten as follows:

$$\begin{aligned} y^I(n) &= s_c^I(n) + b_c^I(n) - b_s^Q(n) \\ y^Q(n) &= s_s^I(n) + b_s^I(n) + b_c^Q(n) \end{aligned} \tag{27}$$

where

$$\begin{aligned} s_c^I(n) &= \cos 2\pi\mu n \cdot s^I(n), \quad s_s^I(n) = \sin 2\pi\mu n \cdot s^I(n) \\ b_c^I(n) &= \cos 2\pi\mu n \cdot b^I, \quad b_s^I(n) = \sin 2\pi\mu n \cdot b^I \\ b_c^Q(n) &= \cos 2\pi\mu n \cdot b^Q, \quad b_s^Q(n) = \sin 2\pi\mu n \cdot b^Q \end{aligned} \tag{28}$$

By substituting $y(n) = y^I(n) + j \cdot y^Q(n)$ into (5), the RX signal $r(n) = r^I(n) + jr^Q(n)$ with impairments can be expressed by

$$\begin{aligned} r^I(n) &= e_1(n) \otimes y^I(n) + e_2(n) \otimes y^Q(n) + d^I \\ r^Q(n) &= e_3(n) \otimes y^I(n) + e_4(n) \otimes y^Q(n) + d^Q \end{aligned} \tag{29}$$

where

$$\begin{aligned} e_1(n) &= h_R^I(n), \quad e_2(n) = 0 \\ e_3(n) &= -\alpha_R \sin\theta_R h_R^Q(n), \quad e_4(n) = \alpha_R \cos\theta_R h_R^Q(n) \end{aligned} \tag{30}$$

Then, by substituting (27) into (29), the RX I and Q signals with impairments can be written as

$$\begin{aligned} r^I(n) &= e_1(n) \otimes \left\{ s_c^I(n) + b_c^I(n) - b_s^Q(n) \right\} \\ &\quad + e_2(n) \otimes \left\{ s_s^I(n) + b_s^I(n) + b_c^Q(n) \right\} + d^I \end{aligned} \tag{31}$$

$$\begin{aligned} r^Q(n) &= e_3(n) \otimes \left\{ s_c^I(n) + b_c^I(n) - b_s^Q(n) \right\} \\ &\quad + e_4(n) \otimes \left\{ s_s^I(n) + b_s^I(n) + b_c^Q(n) \right\} + d^Q \end{aligned} \tag{32}$$

The RX signals in (31) and (32) can be observed by using L_r samples to estimate the real-based parallel impairment parameters. The vector form of the RX signal can be written as

$$\mathbf{r}^I = \begin{bmatrix} \mathbf{1} & \mathbf{S}_c^I & \mathbf{S}_s^I & \mathbf{C} & \mathbf{S} \end{bmatrix} \cdot \mathbf{t}_1 \tag{33}$$

$$\mathbf{r}^Q = \begin{bmatrix} \mathbf{1} & \mathbf{S}_c^I & \mathbf{S}_s^I & \mathbf{C} & \mathbf{S} \end{bmatrix} \cdot \mathbf{t}_2 \tag{34}$$

where $\mathbf{S}_c^I$, $\mathbf{S}_s^I$, $\mathbf{C}$, and $\mathbf{S}$ are the Toeplitz matrices of $s_c^I(n)$, $s_s^I(n)$, $\cos 2\pi\mu n$, and $\sin 2\pi\mu n$, respectively. In (33) and

(34), $\mathbf{t}_1$ and $\mathbf{t}_2$ are the composite impairment vectors, expressed as follows:

$$\mathbf{t}_1 = \left[\, d^I \quad \mathbf{e}_1^T \quad \mathbf{e}_2^T \quad b^I\mathbf{e}_1^T + b^Q\mathbf{e}_2^T \quad b^I\mathbf{e}_2^T - b^Q\mathbf{e}_1^T \,\right]^T \tag{35}$$

$$\mathbf{t}_2 = \left[\, d^Q \quad \mathbf{e}_3^T \quad \mathbf{e}_4^T \quad b^I\mathbf{e}_3^T + b^Q\mathbf{e}_4^T \quad b^I\mathbf{e}_4^T - b^Q\mathbf{e}_3^T \,\right]^T \tag{36}$$

The LS method and FO-based BPSK training signals can be used to estimate each parameter of the composite impairment vectors as follows:

$$\begin{aligned} \hat{\mathbf{t}}_1 &= \mathbf{P}^\dagger \mathbf{r}^I \\ \hat{\mathbf{t}}_2 &= \mathbf{P}^\dagger \mathbf{r}^Q \end{aligned} \tag{37}$$

where $\mathbf{P} = \left[\, \mathbf{1} \ \mathbf{S}_c^I \ \ \mathbf{S}_s^I \ \ \mathbf{C} \ \mathbf{S} \,\right]$ is the composite training matrix.

After the RX impairment parameters are estimated, the postprocessing parameters can be calculated. As displayed in Fig. 3, we propose a symmetric real-based parallel postprocessing calibration design. From the relationship between the postprocessing and impairment parameters, the postprocessing filters $\mathbf{f}_i$, $i = 1, \cdots, 4$ and the post-calibrating DC offset $c^I + jc^Q$ can be determined. To estimate the post-calibrating DC offset, we can refer to the structure in Fig. 3 to obtain the relationship between the post-calibrating DC offset c and RF impairments. This relationship can be expressed as follows:

$$\begin{aligned} d^I \cdot \mathbf{1}^T \cdot \mathbf{f}_1 + d^Q \cdot \mathbf{1}^T \cdot \mathbf{f}_2 + c^I &= 0 \\ d^I \cdot \mathbf{1}^T \cdot \mathbf{f}_3 + d^Q \cdot \mathbf{1}^T \cdot \mathbf{f}_4 + c^Q &= 0 \end{aligned} \tag{38}$$

where $\mathbf{f}_i$, $i = 1, \cdots, 4$, are postprocessing filters with length L. These filters are the vector-form responses of $f_i(n)$. The post-calibrating DC offsets c^I and c^Q can be estimated through matrix operation as follows:

$$\begin{bmatrix} c^I \\ c^Q \end{bmatrix} = -\begin{bmatrix} \sum_{n=0}^{L-1} f_1(n) & \sum_{n=0}^{L-1} f_2(n) \\ \sum_{n=0}^{L-1} f_3(n) & \sum_{n=0}^{L-1} f_4(n) \end{bmatrix} \begin{bmatrix} d^I \\ d^Q \end{bmatrix} \tag{39}$$

Moreover, to estimate the four postprocessing filters according to the proposed calibration structure in Fig. 3, the relationship between the impairment and postprocessing parameters can be expressed as follows:

$$\begin{aligned} &z^I(n) \\ &= f_1(n) \otimes \left(e_1(n) \otimes y^I(n) + e_2(n) \otimes y^Q(n) + d^I \right) \\ &\quad + f_2(n) \otimes \left(e_3(n) \otimes y^I(n) + e_4(n) \otimes y^Q(n) + d^Q \right) + c^I \end{aligned} \tag{40}$$

$$\begin{aligned} &z^Q(n) \\ &= f_3(n) \otimes \left(e_1(n) \otimes y^I(n) + e_2(n) \otimes y^Q(n) + d^I \right) \\ &\quad + f_4(n) \otimes \left(e_3(n) \otimes y^I(n) + e_4(n) \otimes y^Q(n) + d^Q \right) + c^Q \end{aligned} \tag{41}$$

By using the DC cancellation property in (38), the post-processing signal can be rewritten with $y^I(n)$ and $y^Q(n)$ as follows:

$$\begin{aligned} z^I(n) &= (f_1(n) \otimes e_1(n) + f_2(n) \otimes e_3(n)) \otimes y^I(n) \\ &\quad + (f_1(n) \otimes e_2(n) + f_2(n) \otimes e_4(n)) \otimes y^Q(n) \end{aligned} \tag{42}$$

$$\begin{aligned} z^Q(n) &= (f_3(n) \otimes e_1(n) + f_4(n) \otimes e_3(n)) \otimes y^I(n) \\ &\quad + (f_3(n) \otimes e_2(n) + f_4(n) \otimes e_4(n)) \otimes y^Q(n) \end{aligned} \tag{43}$$

For the RX I signal in (42), the $y^I(n)$ signal is retained and $y^Q(n)$ signal is suppressed to cancel out the impairment. Thus,

$$\begin{aligned} f_1(n) \otimes e_1(n) + f_2(n) \otimes e_3(n) &= \delta(n) \\ f_1(n) \otimes e_2(n) + f_2(n) \otimes e_4(n) &= 0 \end{aligned} \tag{44}$$

By using the Toeplitz matrices $\mathbf{E}_i$ of $e_i(n)$, $i = 1, \cdots, 4$ to rewrite the matrix-form equation of (44), the following equation is obtained:

$$\begin{aligned} \mathbf{E}_1 \cdot \mathbf{f}_1 + \mathbf{E}_3 \cdot \mathbf{f}_2 &= \boldsymbol{\delta} \\ \mathbf{E}_2 \cdot \mathbf{f}_1 + \mathbf{E}_4 \cdot \mathbf{f}_2 &= \mathbf{0} \end{aligned} \tag{45}$$

where the vectors $\mathbf{f}_i$, $i = 1, \cdots, 4$, are the response of $f_i(n)$. The LS method can be employed to estimate $\mathbf{f}_1$ and $\mathbf{f}_2$ as follows:

$$\begin{bmatrix} \hat{\mathbf{f}}_1 \\ \hat{\mathbf{f}}_2 \end{bmatrix} = \mathbf{E}^\dagger \begin{bmatrix} \boldsymbol{\delta} \\ \mathbf{0} \end{bmatrix} \quad \text{with } \mathbf{E} = \begin{bmatrix} \mathbf{E}_1 & \mathbf{E}_3 \\ \mathbf{E}_2 & \mathbf{E}_4 \end{bmatrix} \tag{46}$$

Similarly, for the RX Q signal in (43), the $y^Q(n)$ signal is retained and $y^I(n)$ signal is suppressed to avoid impairment effects. Thus, the following equations are obtained:

$$\begin{aligned} f_3(n) \otimes e_1(n) + f_4(n) \otimes e_3(n) &= 0 \\ f_3(n) \otimes e_2(n) + f_4(n) \otimes e_4(n) &= \delta(n) \end{aligned} \tag{47}$$

Then, the composite convolutional matrix $\mathbf{E}$ and the LS method are used to estimate the postprocessing filters $\mathbf{f}_3$ and $\mathbf{f}_4$ as follows:

$$\begin{bmatrix} \hat{\mathbf{f}}_3 \\ \hat{\mathbf{f}}_4 \end{bmatrix} = \mathbf{E}^\dagger \begin{bmatrix} \mathbf{0} \\ \boldsymbol{\delta} \end{bmatrix} \tag{48}$$

To sum up, in this section, we describe the calibration schemes of TX and RX RF impairments. The overall TX/RX calibration flowchart is implemented in the following order: (i) RX RF impairments estimation; (ii) RX RF calibration; (iii) TX RF impairments estimation; (iv) TX RF calibration. Specifically, the RX impairments is first estimated and calibrated by using (25)-(48). The subsequent steps, i.e., TX calibration in (8)-(24), of loopback TX/RX calibration are then performed under the compensated RX scenario. According to the two-step calibration design, we can compensate for the WB RF impairments of the overall transceiver. The proposed scheme can be used to self-calibrate a TX/RX RF IC. We implemented the proposed transceiver calibration schemes in a COST AD9371 TX/RX RF module with impairments (we intentionally turned off the autocalibration function of the AD9371) and Taiwan's ITRI's self-designed RF TX IC module. The schemes exhibited excellent performance in suppressing RF impairments.

IV. SIMULATION AND MEASUREMENT RESULTS

A. SIMULATION RESULTS

A simulation was conducted to test the performance of the proposed real-based parallel filter calibration method for transceivers with WB RF impairments. RX calibration was performed first, followed by TX calibration. The simulation flows are displayed in Fig. 4. For the flow in Fig. 4(a), in which the FO is 1 MHz, RX calibration was performed using the proposed method in Section III-B. Then, for the second flow in Fig. 4(b), the TX calibration method presented in Section III-A was used to compensate for TX RF impairments. Finally, for the flow in Fig. 4(c), single-carrier or OFDM test signals were employed to evaluate the performance of RF impairment suppression. The simulation parameters of the RF impairments are listed in Table 1, including the frequency-independent and frequency- dependent I/Q imbalances, and DC offsets.

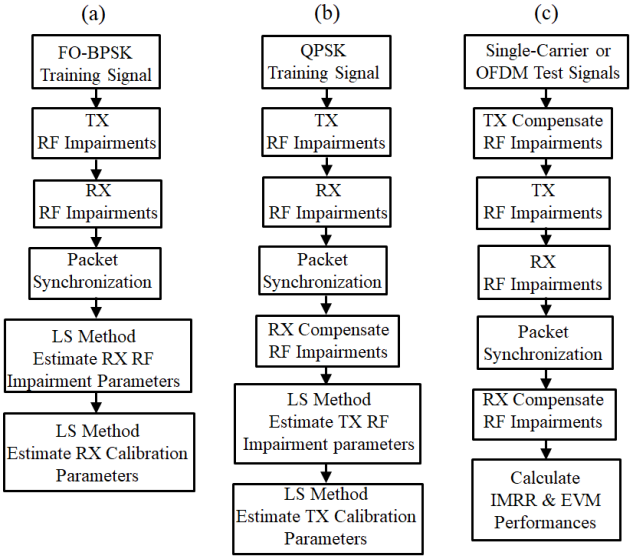

FIGURE 4. Two-step calibration and verification flows of the loopback transceiver. (a) Calibration flow of RX RF impairments. (b) Calibration flow of TX RF impairments. (c) Verification flow through using single-tone and OFDM signals to demonstrate the performance of the proposed two-step calibration flows.

The composite RF impairments were estimated; however, they could not be separated to verify the estimation results of individual impairments. Thus, we examined the suppression performance of the image signals induced by the I/Q imbalance (i.e., IMRR). The IMRR is the ratio of the power of the desired signal to that of the image signal. The IMRRs of TX impairment calibration when using single tones at 20 and 40 MHz for testing are displayed in Figs. 5 and 6, respectively. The IMRRs can confirm the image interference of different tones being calibrated under the same WB compensation parameters. That is, Fig. 5(a) shows that before preprocessing at the TX, the image signal with a frequency of -20 MHz exhibited an IMRR of 13.6422 dB. After the preprocessing calibration depicted in Fig. 5(b), the IMRR improved to 91.7693 dB. Similarly, for the single tone signal at 40 MHz

TABLE 1. RF impairment parameters.

RF Impairments	Parameter Value
Frequency independent I/Q imbalance $(\alpha_T, \theta_T),\ (\alpha_R, \theta_R)$	$(\alpha_T = 0.9,\ \theta_T = 4^\circ)$ $(\alpha_R = 0.7,\ \theta_R = -2^\circ)$
Frequency dependent I/Q imbalance for TX [2] $\{h_T^I(n),\ h_T^Q(n)\}$	$h_T^I(n) = [1\ \ 0.2\ \ 0.1\ \ 0.05]$ $h_T^Q(n) = [0.9\ \ 0.1\ \ 0.08\ \ 0.12]$
Frequency dependent I/Q imbalance for RX $\{h_R^I(n),\ h_R^Q(n)\}$	$h_R^I(n) = [0.95\ \ -0.3\ \ 0.15\ \ -0.08]$ $h_R^Q(n) = [1\ \ -0.2\ \ 0.1\ \ 0.06]$
TX DC offset b And RX DC offset d	$b^I = -0.1,\ b^Q = 0.2$ $d^I = 0.1,\ d^Q = 0.08$

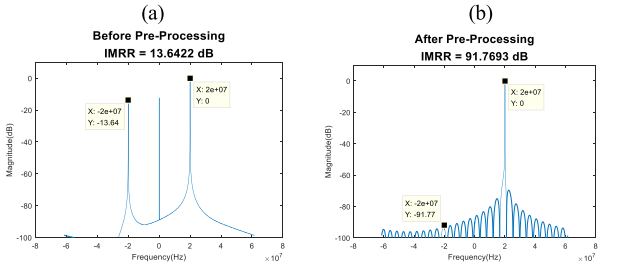

FIGURE 5. Single tone at 20 MHz to verify the calibration performance at the TX: (a) IMRR = 13.6422 dB before preprocessing and (b) 91.7693 dB after preprocessing.

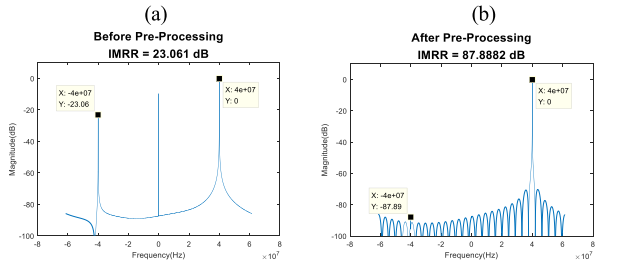

FIGURE 6. Single tone at 40 MHz to verify the calibration performance at the TX: (a) IMRR = 23.061 dB before preprocessing and (b) 87.8882 dB after preprocessing.

displayed in Fig. 6, the improvement in the IMRR is approximately given by 64 dB after preprocessing calibration. The simulation results indicate that the image signal and DC offset can be successfully suppressed by the WB TX calibration schemes.

The IMRRs for RX impairment calibration when using a single tone at 20 and 40 MHz are illustrated in Figs. 7 and 8, respectively. After postprocessing, image signal suppression was achieved at an IMRR of approximately 99.011 dB at 20 MHz and approximately 88.238 dB at 40MHz. Moreover, the DC offsets were cancelled out. Thus, the aforementioned

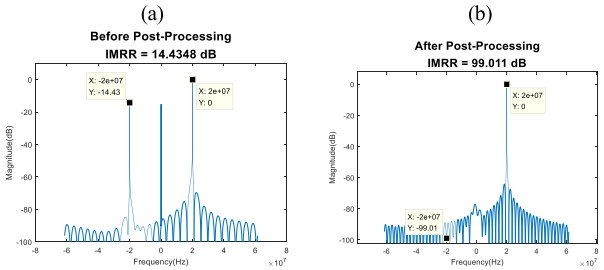

FIGURE 7. Single tone at 20 MHz to verify the calibration performance at the RX: (a) IMRR = 14.4348 dB before postprocessing and (b) 99.011 dB after postprocessing.

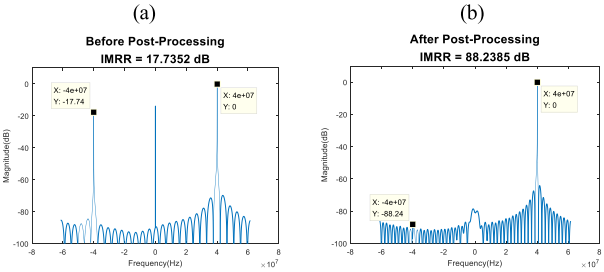

FIGURE 8. Single tone at 40 MHz to verify the calibration performance at RX: (a) IMRR = 17.7352 dB before postprocessing and (b) 88.2385 dB after postprocessing.

simulation results confirm that the proposed methods are useful for the calibration of a WB TX/RX with impairments.

B. MEASUREMENT RESULTS

Besides computer simulation, we also setup an all-digital and software-based testing platform to further verify that the proposed two-step calibration procedure can successfully calibrate the joint TX/RX imperfections of COTS RF modules when configured in loopback transceiver. We employed WB RF modules (i.e., the AD9371 RF module and Taiwan ITRI RF module) and instruments that can integrate the software platform to validate the proposed calibration techniques.

In the first measurement scenario, we set up the AD9371 TX/RX loopback platform with RF impairment effects as displayed in Fig. 9. The measurement flows were the same as those described in Section IV-A (Fig. 4). In the first flow, the AD9371 module transmitted the FO-based BPSK signal with a bandwidth of approximately 60 MHz for RX calibration. For the AD9371 module, we used the following parameters: TX/RX sampling frequency = 122.88 MHz, TX center frequency = 1 GHz, RX center frequency = 995 MHz, and intentional FO = 5 MHz. In the second flow, the AD9371 module transmitted the QPSK signal with a bandwidth of approximately 60 MHz and a TX/RX center frequency of 1 GHz, which was used for TX calibration. Before the aforementioned two TX/RX calibration steps were performed, the AD9371 module with impairments transmitted a single tone at 1010 MHz, which induced an image tone at 990 MHz with an IMRR of 39.32 dB and a DC offset of −45 dBm, as depicted in Fig. 10(a). After TX calibration of the AD9371 module, the image tone was suppressed, with

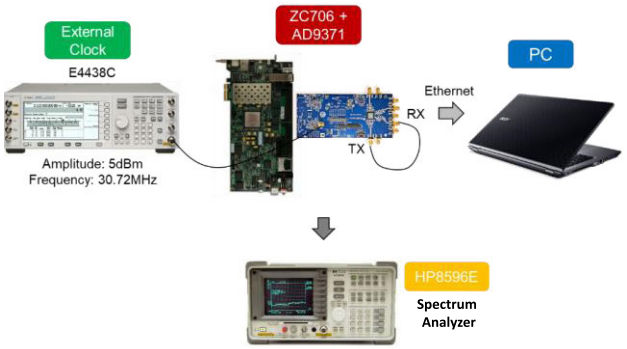

FIGURE 9. Measurement platform of AD9371 TX/RX loopback calibration.

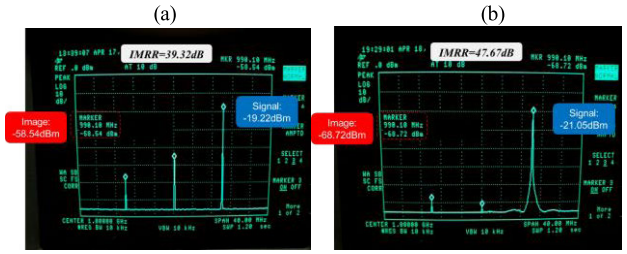

FIGURE 10. Single tone at 1010 MHz to verify the calibration performance for the AD9371 TX module: (a) IMRR = 39.32 dB before preprocessing and (b) 47.67 dB after preprocessing.

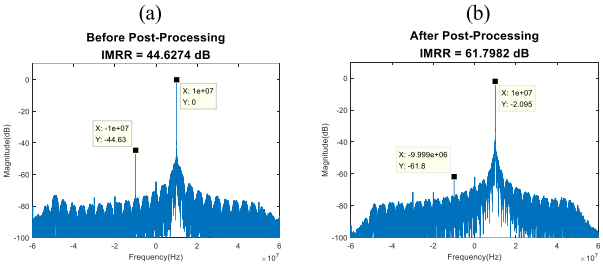

FIGURE 11. Single tone at a frequency of 10 MHz (after down-conversion by a center frequency of 1 GHz) to verify the calibration performance for the AD9371 RX module: (a) IMRR = 44.6274 dB before postprocessing and (b) 61.7982 dB after postprocessing.

IMRR = 47.67 dB and DC offset = −70 dBm, as displayed in Fig. 10(b).

The IMRR of the AD9371 module is increased by about 17 dB after RX postprocessing calibration (Fig. 11). In a multicarrier signal test, the AD9371 module transmitted an OFDM 64QAM signal (Fig. 12), which improved the EVM by approximately 10 dB after TX/RX calibration.

In the second measurement scenario, we set up the ITRI self-designed RF TX module, which is displayed in Fig. 13. The calibration flows were the same as those for the AD9371 module. Because the ITRI module provides only RF TX function, we adopted a Keysight MXG N5182B generator to generate the baseband QPSK training signals with a sampling rate of 200 MHz. The I/Q signals were up-converted to a center frequency of 1 GHz by using the ITRI RF module with impairment effects. Then, an NI PXIe-1075 5646R platform without impairments was employed to down-convert

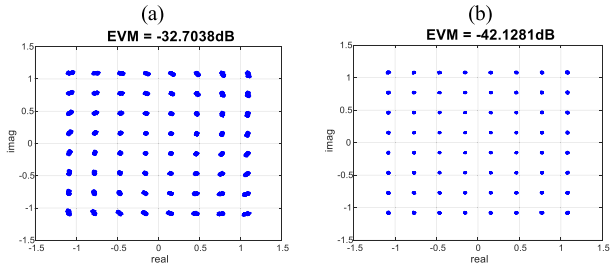

FIGURE 12. OFDM 64QAM signal to verify the loopback calibration performance for the AD9371 TX/RX module: (a) EVM = −32.7038 dB before calibration and (b) −42.1281 dB after calibration.

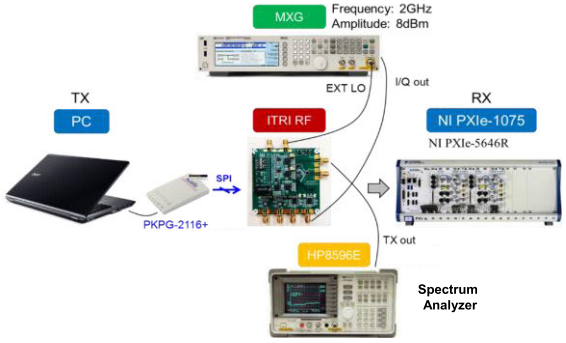

FIGURE 13. Measurement platform of ITRI TX RF calibration.

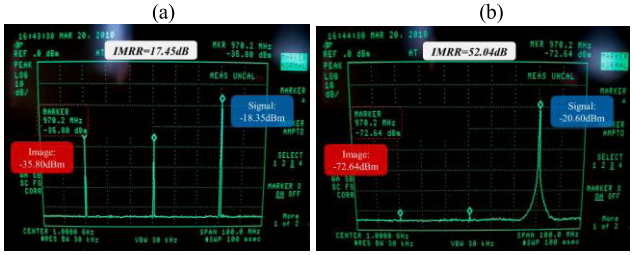

FIGURE 14. Single tone at 1030 MHz to verify the calibration performance for the ITRI TX module: (a) IMRR = 17.45 dB before preprocessing and (b) 52.04 dB after preprocessing.

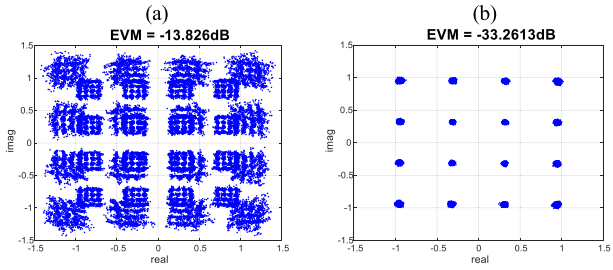

FIGURE 15. OFDM 16QAM signal to verify the calibration performance for the ITRI TX module: (a) IMRR = −13.826 dB before preprocessing and (b) −33.2613 dB after preprocessing.

the ITRI RF signal into an I/Q signal. After the down-conversion, the RX signal was processed using the proposed calibration schemes. After the RF impairment parameters were estimated, we exploited the TX signal tone and multi-carrier signals to test the TX calibration performance. For the single-tone test at 1030 MHz, the proposed method improved the image and DC suppression performance (Fig. 14). The performance improvement in the IMRR and DC offset were approximately 35 and 30 dB, respectively.

For the OFDM 16QAM test signal, the improvement in the EVM was approximately 20 dB after TX preprocessing calibration (Fig. 15). The aforementioned simulation and measurement results confirm that the proposed calibration schemes can overcome WB RF imperfections and achieve high-quality WB communication.

V. CONCLUSION

Frequency-dependent and frequency-independent I/Q imbalances and DC offsets cannot be ignored in WB systems. We propose a real-based parallel structure to estimate and calibrate TX/RX RF impairments. In the proposed two-step calibration (I suggest to use two-stage) procedure, RX calibration is performed before TX calibration. Through both computer simulations and real-world experiments, the proposed method is shown to successfully mitigate the joint TX/RX WB RF impairments and considerably improve such performance indices as IMRR, DC offsets, and EVM.

As for the future research directions, the proposed calibration techniques of I/Q imbalance and DC offsets can be extended to the cases with other impairments [16], e.g., broad bandwidth I/Q imbalance [17], PA nonlinear distortion [18], [19], time-varying DC [18]–[21], and MIMO coupling [14]. It is noteworthy that the proposed calibration techniques in this paper only consider the TX/RX RF I/Q imbalance and DC offset effects. The other distortion effects are out of the design scope of this paper. For the future research issue of time-varying DC, i.e., adopting the time-varying DC model in [20], [21], the parameters of the time-varying DC offset can be estimated and calibrated by the proposed design flow in this paper. For the purpose of training sequence design in this paper, the frequency offset BPSK and QPSK training signals are designed for the RF calibrations of the receiver and transmitter sides, respectively, which can achieve the TX/RX loopback calibration. It is similar to the work in [2] which designed the optimal training sequences for TX/RX loopback calibration. However, it is different from [22], in which the blind method was proposed only for the RF calibration at the receiver side. For the training-based approaches, the calibration is performed at the offline mode, which does not occupy any resource at the online communication mode, while the training-based approaches are generally more reliable than the blind approaches. For a broader bandwidth, e.g., 1 GHz, the proposed calibration technique with the larger size of the widely-linear filters can be designed to compensate the distortion of the broadband frequency dependent I/Q imbalance. The assumption of the larger size of widely-linear filters is due to a higher sampling rate induced by broadband bandwidth signals, which is similar to the design of the pre-compensation filters in [17]. Moreover, for the multiple impairments effect, the cascaded calibrations, e.g., real-based parallel filters, decoupling, and digital pre-distortion, can be designed to compensate the I/Q imbalance,

TABLE 2. Comparison of the problem scope between this work and others.

	Proposed	[2]	[14]	[17]	[19]	[20]	[22]
TX Preprocessing	V	V	V	V			
RX Postprocessing	V	V			V	V	V
TX/RX IQI/DC Loopback	V	V					
Training (T) or Blind (B)	T	T	T	T	T	T	B
Nonlinear PA (NL-PA)			V		V		
Fixed DC (F-DC) or Time-Varying DC (TV-DC)	F-DC	F-DC	F-DC			TV-DC	
Bandwidth (MHz)	60	20	20	1000	50	20	10
MIMO Coupling			V				
Measurement Verification	V			V	V		
Future Research	NL-PA+ Coupling + TV-DC						

coupling, and nonlinear impairments, respectively. Finally, we provide a comparison table to summarize the state of the art in RF impairments calibration in order to highlight the possible future research issues related to this work, which is shown in Table 2.

ACKNOWLEDGMENT

The authors would like to thank the anonymous reviewers for their valuable comments, which increased the quality of the paper. They appreciated Wallace academic editing for his editorial assistance. They are also grateful to the ITRI in Taiwan for technical support regarding the WB 5G RF module.

REFERENCES

[1] W. Li, Y. Zhang, L.-K. Huang, J. Cosmas, C. Maple, and J. Xiong, "Self-IQ-Demodulation based compensation scheme of frequency-dependent IQ imbalance for wideband direct-conversion transmitters," *IEEE Trans. Broadcast.*, vol. 61, no. 4, pp. 666–673, Dec. 2015.

[2] C.-J. Hsu and W.-H. Sheen, "Joint calibration of transmitter and receiver impairments in direct-conversion radio architecture," *IEEE Trans. Wireless Commun.*, vol. 11, no. 2, pp. 832–841, Feb. 2012.

[3] L. Ding, Z. Ma, D. R. Morgan, M. Zierdt, and G. Tong Zhou, "Compensation of frequency-dependent Gain/Phase imbalance in predistortion linearization systems," *IEEE Trans. Circuits Syst. I, Reg. Papers*, vol. 55, no. 1, pp. 390–397, Feb. 2008.

[4] Y. Li, *In-Phase and Quadrature Imbalance Modeling, Estimation, and Compensation*. New York, NY, USA: Springer, 2013.

[5] Y. Luo, W. Li, and X. Hou, "A joint estimation and independent compensation scheme for transmitter and receiver IQ imbalance in zero-IF transceivers," in *Proc. IEEE Int. Conf. Comput. Electromagn. (ICCEM)*, Mar. 2019, pp. 1–5.

[6] A. Khandelwal and A. Verma, "A novel gain, phase and offset calibration scheme for wideband direct-conversion transmitters," in *Proc. IEEE 81st Veh. Technol. Conf. (VTC Spring)*, May 2015, pp. 1–5.

[7] X. Zhang, H. Li, W. Liu, and J. Qiao, "Iterative IQ imbalance compensation receiver for single carrier transmission," *IEEE Trans. Veh. Technol.*, vol. 66, no. 9, pp. 8238–8248, Sep. 2017.

[8] M. Matsui, T. Nakagawa, R. Kudo, K. Ishihara, and M. Mizoguchi, "Blind frequency-dependent IQ imbalance compensation scheme using CMA for OFDM system," in *Proc. IEEE 22nd Int. Symp. Pers., Indoor Mobile Radio Commun.*, Toronto, ON, Canada, Sep. 2011, pp. 1386–1390.

[9] E. Lopez-Estraviz, S. De Rore, F. Horlin, A. Bourdoux, and L. Van der Perre, "Pilot design for joint channel and frequency-dependent transmit/receive IQ imbalance estimation and compensation in OFDM-based transceivers," in *Proc. IEEE Int. Conf. Commun.*, Glasgow, U.K., Jun. 2007, pp. 4861–4866.

[10] J. K. Cavers and M. W. Liao, "Adaptive compensation for imbalance and offset losses in direct conversion transceivers," *IEEE Trans. Veh. Technol.*, vol. 42, no. 4, pp. 581–588, Nov. 1993.

[11] A. G. K. C. Lim, V. Sreeram, and G.-Q. Wang, "Digital compensation in IQ modulators using adaptive FIR filters," *IEEE Trans. Veh. Technol.*, vol. 53, no. 6, pp. 1809–1817, Nov. 2004.

[12] R. Marchesani, "Digital precompensation of imperfections in quadrature modulators," *IEEE Trans. Commun.*, vol. 48, no. 4, pp. 552–556, Apr. 2000.

[13] L. Anttila, P. Handel, and M. Valkama, "Joint mitigation of power amplifier and I/Q modulator impairments in broadband direct-conversion transmitters," *IEEE Trans. Microw. Theory Techn.*, vol. 58, no. 4, pp. 730–739, Apr. 2010.

[14] F. Gregorio, J. Cousseau, S. Werner, T. Riihonen, and R. Wichman, "Power amplifier linearization technique with IQ imbalance and crosstalk compensation for broadband MIMO-OFDM transmitters," *EURASIP J. Adv. Signal Process.*, vol. 2011, no. 1, pp. 1–15, Jul. 2011.

[15] Z. A. Khan, E. Zenteno, P. Handel, and M. Isaksson, "Digital predistortion for joint mitigation of I/Q imbalance and MIMO power amplifier distortion," *IEEE Trans. Microw. Theory Techn.*, vol. 65, no. 1, pp. 322–333, Jan. 2017.

[16] M. Valkama, A. Springer, and G. Hueber, "Digital signal processing for reducing the effects of RF imperfections in radio devices—An overview," in *Proc. IEEE Int. Symp. Circuits Syst.*, May 2010, pp. 813–816.

[17] A. Rezola, J. F. Sevillano, D. Del Rıo, I. Guruceaga, R. Berenguer, and I. Vélez, "Frequency-selective IQ imbalance in zero-second-IF transceivers for wide-band mmW links," *Int. J. Commun.*, vol. 9, pp. 98–104, Jul. 2015.

[18] G. Hueber, Y. Zou, K. Dufrene, R. Stuhlberger, and M. Valkama, "Smart front-end signal processing for advanced wireless receivers," *IEEE J. Sel. Topics Signal Process.*, vol. 3, no. 3, pp. 472–487, Jun. 2009.

[19] M. Grimm, M. Allen, J. Marttila, M. Valkama, and R. Thoma, "Joint mitigation of nonlinear RF and baseband distortions in wideband direct-conversion receivers," *IEEE Trans. Microw. Theory Techn.*, vol. 62, no. 1, pp. 166–182, Jan. 2014.

[20] T. Liu and H. Z. Li, "Carrier frequency offset estimation for OFDM systems with time-varying DC Offset," *EURASIP J. Adv. Signal Process.*, vol. 2012, Jul. 2012, Art. no. 156, doi: 10.1186/1687-6180-2012-156.

[21] U. Yunus, H. Lin, and K. Yamashita, "Joint estimation of carrier frequency offset and IQ imbalance in the presence of timing-varying DC offset," *IEICE Trans. Communun.*, vol. E93-B, no. 1, pp. 16–21, Jan. 2010.

[22] L. Anttila, M. Valkama, and M. Renfors, "Blind compensation of frequency-selective I/Q imbalances in quadrature radio receivers: Circularity-based approach," in *Proc. IEEE Int. Conf. Acoust., Speech Signal Process. (ICASSP)*, Apr. 2007, pp. III-245–III-248.

JUINN-HORNG DENG (Member, IEEE) received the Ph.D. degree in communications engineering from National Chiao Tung University, Taiwan, in 2003. From 2003 to 2008, he was with the Electronic System Research Department, Chung Shan Institute of Science Technology, Taiwan. In 2008, he joined the Faculty of Yuan Ze University, Chungli City, Taiwan, where he is currently a Professor with the Department of Electrical Engineering. From July 2010 to September 2010, he had been invited to join the Hawaii Center for Advanced Communications (HCAC), College of Engineering, University of Hawaii at Manoa, as a Visiting Research Scholar, doing research on hybrid smart antennas for wireless communications. He is currently the Vice Director of the Communication Research Center (CRC), Yuan Ze University. His research interests include smart antennas, transceiver design, RF calibration, communication signal processing, communication circuit design, and MIMO techniques for wireless communications. He has published over 60 papers and holds six US patents.

CHIA-FANG LEE was born in Miaoli, Taiwan, in 1994. She received the master's degree in electrical engineering from Yuan Ze University, Chungli, Taiwan, in 2016. Her current research interests include RF calibration, wireless communications, and software-defined radios.

MENG-LIN KU (Member, IEEE) received the B.S., M.S., and Ph.D. degrees from National Chiao Tung University, Hsinchu, Taiwan, in 2002, 2003, and 2009, respectively, all in communication engineering. From 2009 to 2010, he was a Postdoctoral Research Fellow of the Department of Electrical and Computer Engineering, National Chiao Tung University, under the supervision of Prof. L.-C. Wang, and also with the School of Engineering and Applied Sciences, Harvard University, under the supervision of Prof. V. Tarokh. In August 2010, he became a Faculty Member of the Department of Communication Engineering, National Central University, Jungli, Taiwan, where he is currently a Professor. During the Summer of 2013, he was a Visiting Scholar at the Signals and Information Group of Prof. K. J. Ray Liu, University of Maryland. His current research interests are in the areas of green communications, cognitive radios, and optimization and learning for radio access. He was a recipient of the Best Counseling Award, in 2012, and the university-level Best Teaching Award, in 2014, 2015, and 2016, and the Research Excellence Award, in 2018, 2019, and 2020, respectively, all at National Central University. He was a recipient of the Exploration Research Award of the Pan Wen Yuan Foundation, in 2013, and the Chinese Institute of Electrical Engineering Outstanding Young Electrical Engineer Award, in 2019. He is also serving as an Associate Editor of IEEE Access.

JENG-KUANG HWANG (Senior Member, IEEE) was born in Taipei, Taiwan, in 1962. He received the graduation degree (Hons.) in electrical engineering from the National Taipei Institute of Technology, Taipei, in 1982, and the Ph.D. degree in electrical engineering from National Tsing Hua University, Hsinchu, Taiwan, in 1991. Since 1991, he has been with the Department of Electrical Engineering and the Department of Communication Engineering, Yuan Ze University (YZU), Zhongli, Taiwan. In 1997, he had been a Visiting Professor with AT&T Labs/Research, Florham Park, NJ, USA. From 2008 to 2011, he has served as the Chairman of the Communication Engineering Department, YZU, where he is currently the Director of the Communication Research Center. He has conducted many research projects in both academia and industry, authored or coauthored over 150 papers and two books, and holds 20 patents. His current research interests include communication signal processing, software-defined radios, signal measurement and instrumentation, MIMO channel sounding and modeling, and radar systems.